Optical Materials 109 (2020) 110281

Contents lists available at ScienceDirect

Optical Materials

journal homepage: http://www.elsevier.com/locate/optmat

A novel leaves and needles like TiO_2 (LNT) electron transfer layer (ETL) as an alternative to meso-porous TiO_2 electron transfer layer (ETL) in perovskite solar cell

Hamid Latif [a,*], Zuha Azher [a], Syeda Ammara Shabbir [a], Saba Rasheed [a], Erum Pervaiz [b], Abdul Sattar [c], Ayesha Imtiaz [d]

[a] Department of Physics, Forman Christian College, Lahore, Pakistan
[b] Chemical Engineering Department, School of Chemical and Materials Engineering (SCME), National University of Sciences and Technology (NUST), Sector H-12, Islamabad, 44000, Pakistan
[c] Physics Department, COMSATS University Islamabad, Lahore Campus, Lahore, Pakistan
[d] Department of Chemistry, Minhaj University, Lahore, Pakistan

ARTICLE INFO

Keywords:
Perovskite solar cell
Electron transport layer
Hole transport layer
Titanium dioxide

ABSTRACT

Two perovskite solar cells one with leaves and needles like TiO_2 (LNT) and other with meso-porous TiO_2 as electron transfer layer (ETL) were fabricated. The perovskite solar cell structure FTO/Compact-TiO_2/LNT/$CH_3NH_3PbBr_3$/Spiro-OMeTAD/Ag with leaves and needles like TiO_2 electron collector, exhibit high efficiency up to 9% being supported by high open-circuit voltage and fill factor up to 0.8 V and 0.89, respectively. The second perovskite solar cell structure FTO/Compact-TiO_2/Meso-porous TiO_2/$CH_3NH_3PbBr_3$/Spiro-OMeTAD/Ag with meso-porous TiO_2 electron collector, efficiency is 6.2% with open-circuit voltage and fill factor up to 0.77 V and 0.71 respectively. As compared to meso-porous TiO_2 electron collector layer, leaves and needles like TiO_2 has better electron band alignment with compact TiO_2 as hole blocking layer and hence, results in higher efficiency.

1. Introduction

Organic-inorganic halide perovskite solar cells (PSCs) are rapidly emerging renewable energy sources in the world of photovoltaics, owing to their advantages such as low cost easy fabrication, use of light weight flexible substrates and PCE exceeding 25.2% [1,2]. Perovskite (ABX3, where A is organic, B is inorganic and X3 is trihalide) material has received remarkable interest due to long diffusion length (up to 175 μm), high charge carrier mobility, high absorbance coefficient (10^3 cm^{-1}) in complete visible solar spectrum, low band gap range (1.5–2.3eV), low binding energy, long diffusion lengths for photo-generated carriers and ambipolar transport behavior [3].

Perovskite layer acting as light absorbent is sandwiched between n-type electron transporting layer (ETL) and p-type hole transporting layer (HTL). To obtain efficient devices, choice of these charge selective contacts depends upon some stringent requirements such as selection of material, structure, and ample energy level alignment. Among the different ETL materials (ZnO, Al_2O_3, PCBM, CdSe, Zn_2SnO_4, CdS, SnO_2, etc.) introduced in PSCs, TiO_2 is still grasping the efficiency record [4]. TiO_2 is widely used in photovoltaic technologies due to its good optical properties, photostability, high electron mobility, suitable band structure, chemical stability, corrosion resistance, non-toxicity, and simple fabrication [5]. Surface morphological characteristics of TiO_2 are closely related with photocatalytic efficiencies. Various nano structures of TiO_2 such as nano rods, nano spheres, nanotubes, nanowires and mesoporous have been implemented as ETL. Among different structural morphologies one dimensional structure like TiO_2 nanotubes (TNTs) and TiO_2 nano rods (TNR) can be an attractive approach to enhance charge transfer hence increasing the PCE. These structures have been widely explored due to easy fabrication process and outstanding properties. These structures provide 1D transportation path to electrons which not only increases the charge transfer rate but also hinders the charge recombination [6,7]. Due to these outstanding properties of superior charge transport, high scattering and high absorption of light 1D nanostructures have been used as ETL [8–15]. Hence deposition of 1D TiO_2 as ETL increased charge transportation and showed better device performance [16,17].

Different strategies have been used to increase the solar energy

* Corresponding author.
E-mail address: hamidlatif@fccollege.edu.pk (H. Latif).

https://doi.org/10.1016/j.optmat.2020.110281
Received 14 February 2020; Received in revised form 1 June 2020; Accepted 27 July 2020

conversion. One of these approaches is to increase the surface area by developing more active sites to enhance the capability of light scattering and trapping. The morphology of TiO_2 also plays an important role for enhancement in light harvesting. Branched structures show better ability to scatter and trap light because of high surface area [17–20]. On the other hand, leave like structures can also been used to enhance trapping of light which can also contribute in increase of PCE [21].

Granular nano-disks like structures of amorphous titanium dioxide synthesized using simple technique of anodiztion of porous titanium foam show excellent photo-electrocatalytic properties and photo-electric conversion. Better photo-electrochemical performance can be attributed to high surface area of titanium (Ti) foam and multiple active adsorption-sites of titanium dioxide nano-disks [22]. Photo-electrode based on flexible three dimensional (3D) nanotubes of TiO_2 prepared by anodization of titanium (Ti) mesh showed low interface impedance and photocurrent of 1.63 $mAcm^{-2}$. This type of photo-electrode based on novel 3D nanotubes of TiO_2 have application in solar cells. Bi_2S_3/-TiO_2 nanotubes based photo-electrode show excellent photo-electrochemical properties with 5.99 $mAcm^{-2}$ photo-current density [23,24].

Several methods available for fabricating 1D structures includes electrochemical anodization, micro-wave irradiation, template method, sol gel method, hydrothermal method, sonoelectrochemical, and alkaline synthesis. Among all these methods electrochemical anodization is widely used cost effective technique. Advantageous characteristics include controllable growth (controlled by anodization parameters), production of strong adhesive nanotubes, and feasibility to tune size and shape of nanotubes to required dimensions [25].

In this research work, leave and needle like structures of TiO_2 (LNT) have been grown as ETL by electrochemical anodization process. A compact layer of TiO_2 is deposited between FTO layer and LNT. Methylamine lead bromide ($CH_3NH_3PbBr_3$) used as perovskite layer shows better stability under heat and moisture [26]. 2,20,7,70tetrakis (N, *N*-di-*p*-ethoxyphenylamino)-9,90-spirobifluorene (Spiro-OMeTAD) as HTM and silver conducting paste as electrode is used. Compact TiO_2 also known as blocking layer is an important component of high efficiency perovskite solar cells [27]. It helps to prevent charge recombination which can take place between perovskite layer and FTO. This charge recombination must be prohibited as it leads to lower charge collection efficiency [9]. Then this device was compare with another device having meso-porous TiO_2 layer instead of LNT layer. All other layers were kept same in both devices just to compare the effect of leaf and needle like structure.

2. Experimental

2.1. Deposition of TiO_2 compact layer

To deposit TiO_2 compact thin film on FTO glass a precursor solution of 0.15 M of titanium isopropoxide in ethanol was stirred for 1 h. The solution was spin coated on glass substrate at 3000 rpm for 30s. The film was thermally annealed at 450°c for 2 h [28].

2.2. Deposition of leaves and needles like TiO_2

For the deposition of leaves and needles like TiO_2 (LNT) two-electrode configuration was used, with compact TiO_2 coated FTO as the working electrode and graphite as the counter electrode in electrochemically anodization at 20 V for 10 min at room temperature. 0.3 g ammonium fluoride was mixed in ethylene glycol and 2 ml DI water was used as electrolyte solution. The sample was rinsed in DI water to remove the electrolyte and then dried in air after anodization. To convert amorphous LNT into anatase phase thermal annealing was done at 450 C for 3 h. For better cell performance, the LNT was also treated in 7.587 g of $TiCl_4$ (aqueous solution) at 70 C for 10 h and then rinsed with ethanol and DI water.

2.3. Deposition of meso-porous titanium dioxide (TiO_2)

TiO_2 paste (Dyesol 18 NR-T) was diluted in ethanol at 1:35 by weight. The solution was spin coated at 2000 rpm for 50s and heated at 500 C for 30 min [29].

2.4. Deposition of methylamine bromide ($CH_3NH_3PbBr_3$)

Methyl amine (40% in methanol) was mixed with hydrobromic acid (48% in water) under continuous stirring for 2 h in 1:1 M ratio to prepare CH_3NH_3Br. The solution was then heated for 24 h at 60 °C in vacuum oven. After that lead bromide $PbBr_2$ and methyl ammonium bromide CH_3NH_3Br were mixed in equi-molar ratio in dimethylformamide (DMF) to prepare $CH_3NH_3PbBr_3$ 40% weight followed by 1 h stirring. The prepared solution was spin coated at 500 rpm for 5s and then at 3000 rpm for 30s. Deposited film was heated at 150 °C for 15 minutes to get dark orange color [30,31].

2.5. Deposition of 2,20,7,70-tetrakis(N,N-di-p-ethoxyphenylamino)-9,90-spirobifluorene (Spiro-OMeTAD)

A hole transporting layer (HTL) was deposited via spin-coating of mixture of Spiro-OMeTAD in Dimethyl formamide DMF (120 mg/ml) at 1000 rpm for 9s and then 4000 rpm for 30s. The prepared sample was then dried at 120 °C for 15 minutes [32].

2.6. Deposition of silver (Ag) electrode

Finally, as top most layer silver was deposited using doctor blade method and dried on hot plate.

After fabrication both devices were analyzed using different characterization techniques. The crystal structure and surface morphology was examined by x ray diffractometer (XRD), transmission electron microscope (TEM) and scanning electron microscopy (SEM). The ultraviolet visible absorption spectra were recorded using spectrophotometer. Localized conductivity of leaves and needle like TiO_2 layer and meso-porous TiO_2 layer was measured with scanning tunneling microscope (STM), EIS analysis was done to find out resistance between interfacial charge transport and charge transfer processes. Solar simulator was used for efficiency analysis.

3. Results and discussion

3.1. Morphology and structural studies

Fig. 1 (a) and (c) shows the SEM micrographs of LNT TiO_2 and meso-porous TiO_2 respectively. Fig. 1 (b) and (d) shows XRD pattern of LNT TiO_2 and meso-porous TiO_2 respectively.

The SEM image in Fig. 1(a) reveals the formation of leaves and needles like structures. Both leaves and needles like structures show no specific alignment. Needles are randomly dispersed among the leaves. This needles and leaves like morphology increases the surface area and area of contact with other layers and thus improves the optical properties like absorbance [33]. SEM micrograph in Fig. 1(c) confirms the formation of mesoporous structure. There are few empty spaces between the particles appear as dark areas in SEM image. Moreover, clusters of particles exist due to agglomeration of particles during synthesis process. Particle size is not uniform throughout the structure. The meso-porous layer plays a vital role to transport electrons from perovskite to external circuit through its conduction band [33].

XRD diffractogram in Fig. 1(b) confirms the formation of TiO_2. There is one high intensity peak at two theta position of 24.8° and its corresponding (hkl) values are (101). This suggests that LNT TiO_2 has grown preferentially with (101) plane that is parallel to FTO substrate [7]. Two other prominent peaks with relatively low intensity are obtained by diffraction from (200) and (211) planes at two theta position of 48.2°

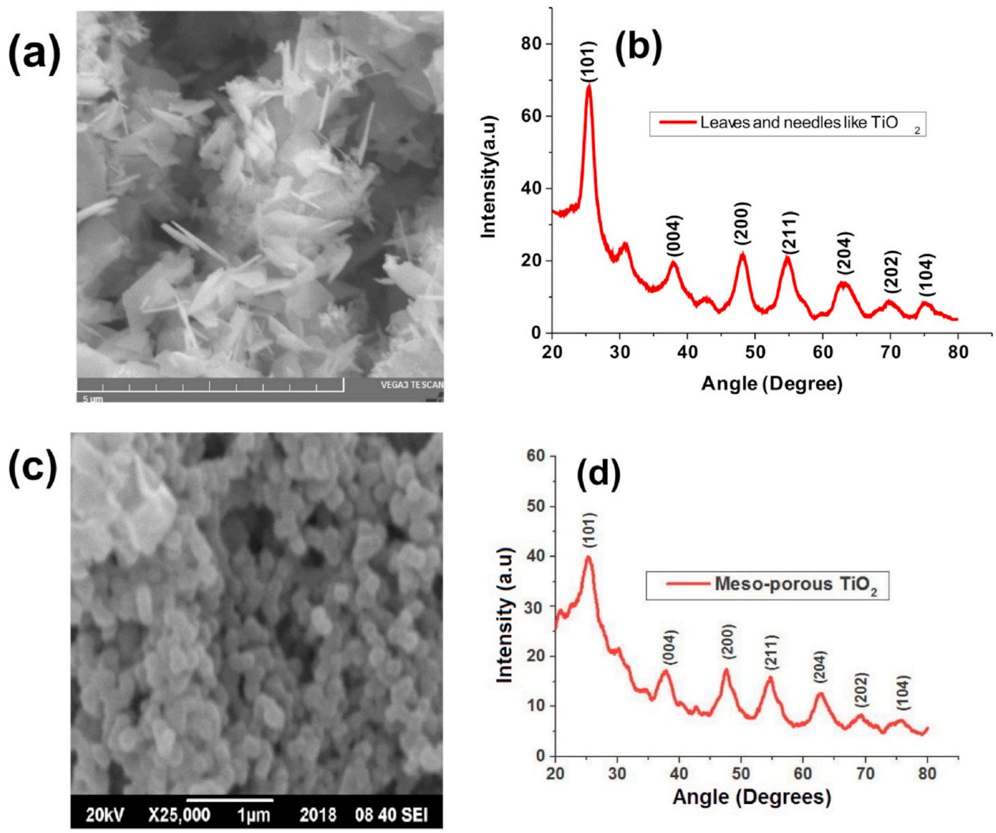

Fig. 1. SEM images of along with XRD profiles of TiO_2 at ETL on compact TiO_2 coated FTO substrate (a) SEM micrograph Leaves and Needle like TiO_2 (LNT) (b) XRD profile of the Leaves and Needle like TiO_2 (LNT) (c) SEM image Meso-porous TiO_2 and (d) XRD pattern of.

and 55.1° respectively. Besides this, there are four other low intensity peaks at two theta positions of 37.8°, 62.9°, 70° and 75.1° with hkl values (004), (204), (202) and (104) respectively. XRD pattern in Fig. 1 (d) shows the peaks due to diffraction from (101), (004), (200), (211), (204), (202) and (104) planes corresponding to the two theta values of 26°, 37.8°, 47.8°, 49.7°, 63°, 69.8° and 76.2° respectively. All the peaks have very low intensity except the one obtained at (101) plane. It may indicate the preferential growth of mesoporous TiO_2 in this direction [7]. The peak broadening is due to the porous structure of TiO_2. XRD pattern has confirmed the formation of TiO_2.

In Fig. 2(a), SEM micrographs of all the layers FTO, compact TiO_2, LNT TiO_2, perovskite and spiro arranged according to device assembly. Similarly, Fig. 2(b) exhibits SEM micrographs of all layers i.e. FTO, compact TiO_2, mesoporous TiO_2, perovskite and spiro. These SEM images are arranged in layers one above the other following the device architecture.

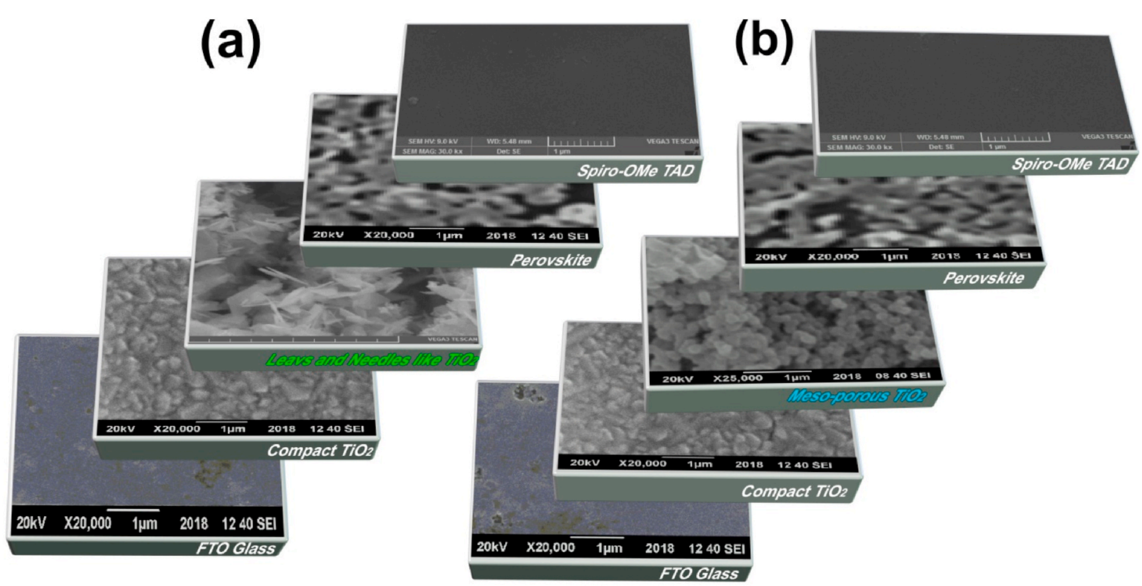

Fig. 2. SEM images of all layers as arranged in both solar cells having all identical layers except electron transport layer (ETL) (a) leaves and needle like TiO_2 as ETL (b) Meso-porous TiO_2 as ETL.

To gain more insight into morphological study of resulting leaves and needles like structures of TiO_2 transmission electron microscopy (TEM) measurements were carried out. TEM images of leaves and needles like structures of TiO_2 are shown in Fig. 3(a) and 3(b).

One dimensional structures shown in Fig. 3(a) are the needles while Fig. 3(b) reveals the presence of randomly oriented leave like nano structures of TiO_2. These leave like structures are of TiO_2 crystals are of different sizes and there are few empty spaces between them.

The scanning tunneling microscopy (STM) was performed and STM images of particle and needle like structures of TiO_2 are presented in Fig. 4(a) and 4(b) and their corresponding IV curves obtained are shown in Fig. 4(c).

The diameter of a TiO_2 particle calculated from STM image is 187 nm. The length and diameter of TiO_2 needle is 137 nm and 39 nm respectively. From IV curves it is observed that both needle and particle structures of TiO_2 exhibit semiconducting behavior. The maximum current of 28 nA can be detected under voltage bias up to 1 V for TiO_2 particle. For TiO_2 needle structure maximum current of 84 nA can be detected.

The electrical conductivity for both was calculated using STM analysis. For TiO_2 particle the conductivity is 0.02 $Ohm^{-1}cm^{-1}$ while conductivity of TiO_2 needle is 0.88 $Ohm^{-1}cm^{-1}$. The electron mobility was also calculated for both particle and needle like structure of TiO_2. The mobility of needle like structure is 5.56×10^{18} cm^2V^{-1}. Whereas for particle like structure the electron mobility is 1.54×10^{17} cm^2V^{-1}. So it is obvious that electrical conductivity and electron mobility of TiO_2 particle is less than that of TiO_2 needle. The better conductivity of needle like structure of TiO_2 will play an important role to improve the efficiency of solar cell.

3.2. Optical and elecrochemical impedance spectroscopic analysis

Fig. 5 shows the UV–Visible absorption spectra of both LNT and mesoporous TiO_2 ETL based solar cells. It is obvious from the figure that both devices show broad absorption in visible range. LNT TiO_2 based solar cell shows maximum absorption in 500 nm–700 nm range. While mesoporous TiO_2 based solar cell has maximum absorption in 400 nm–600 nm range. The maximum absorption for LNT TiO_2 based device is 0.42 at wavelength 524 nm while mesoporous TiO_2 based device has maximum absorption 0.14 at wavelength 402 nm. LNT TiO_2 based solar cell exhibit stronger absorption than mesoporous TiO_2 based solar cell which implies its ability to be photo-activated under irradiation of visible light.

The increased absorption of LNT TiO_2 based solar cell is due to better light trapping characteristics of leaves and needle like structure of TiO_2. Such structure maximizes scatter efficiency and reflectance capability in entire visible region. This results in multiple absorption of incident light. When light falls, it bounces back and forth multiple times and then eventually absorbed. It is beneficial in photon capturing and enhances light harvesting efficiency [21]. The enhanced photocatalytic behavior is attributed to larger surface area and active surfaces which allow them to absorb more incident light [34].

One dimensional structures are considered as an appropriate scaffold to composite with other nanostructures such as nanoparticles, nanosheets etc. To increase surface area and to minimize charge recombination. High surface area of 1D needle like structures of TiO_2 provides active sites to increase capability of light scattering and trapping. Combination of one dimensional needle like structures and leaves like structures increase the surface area and thus scattering and trapping of light [20,35–38]. So the improved optical behavior due to high scattering and absorption of light will contribute to high efficiency.

3.2.1. Electrochemical impedance spectroscopy (EIS)

Electrochemical impedance spectroscopy is an important tool to understand dynamics of interfacial charge transport and charge transfer processes.

Electrochemical impedance spectra were obtained for both mp-TiO_2 and LNT-TiO_2 structures based solar cells. The corresponding Nyquist plots with alternating current (AC) amplitude of 10 mV and frequency range of 10^{-1} to 10^5 Hz are displayed in Fig. 6.

It can be observed from Fig. 6 that only one semi-circle is obtained for these devices. Solar cell based on leaves and needle like structure of TiO_2 has smaller arc so it shows low interface resistance and fast transfer of charge carriers [39]. Mesoporous TiO_2 structure based solar cell has more interface resistance and slow charge transfer. Recombination resistance calculated from Nquist plots for both devices. For mesoporous TiO_2 structure based device the recombination resistance is 993.511 Ω. Whereas recombination resistance calculated for leaves and needle like TiO_2 structure based solar is less i.e. 938.85 Ω.

The low interfacial resistance and fast carrier transport in leaves and needle like TiO_2 structure based device can contribute to achieve better efficiency.

3.3. Device performance

Fig. 7 shows the energy levels of TiO_2, $CH_3NH_3PbBr_3$ and spiro-OMeTAD. It can be seen from this figure that the conduction band (CB) of TiO_2 and $CH_3NH_3PbBr_3$ lies at −4.0 eV and −3.38 eV respectively. This difference of ~0.6 eV between conduction bands provides the required charge separation driving force for collection of electrons.

The valence band (VB) of $CH_3NH_3PbBr_3$ lies at −5.69 eV and highest occupied molecular orbital (HOMO) of spiro-OMeTAD is located at −5.2 eV. Therefore, holes can be easily moved from valence band of $CH_3NH_3PbBr_3$ to highest occupied molecular orbital (HOMO) of spiro-

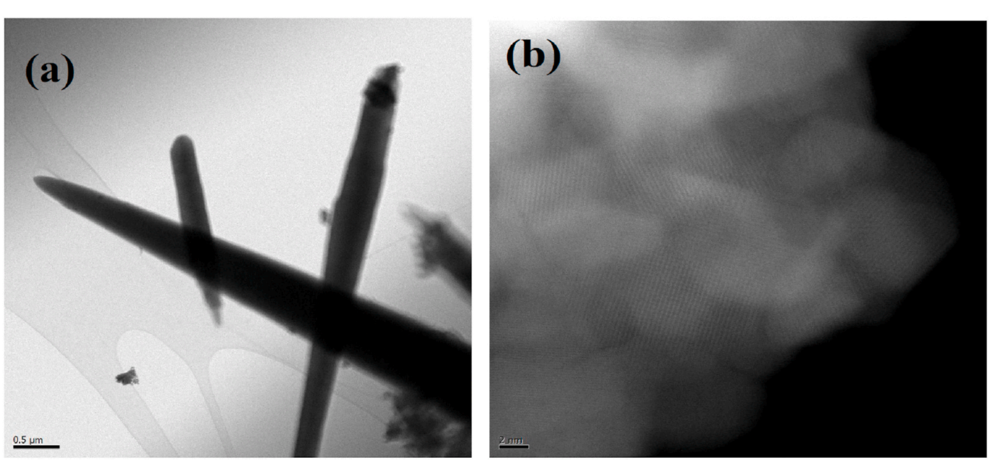

Fig. 3. TEM images of **(a)** needle like structure of TiO_2 **(b)** leaves like structure of TiO_2.

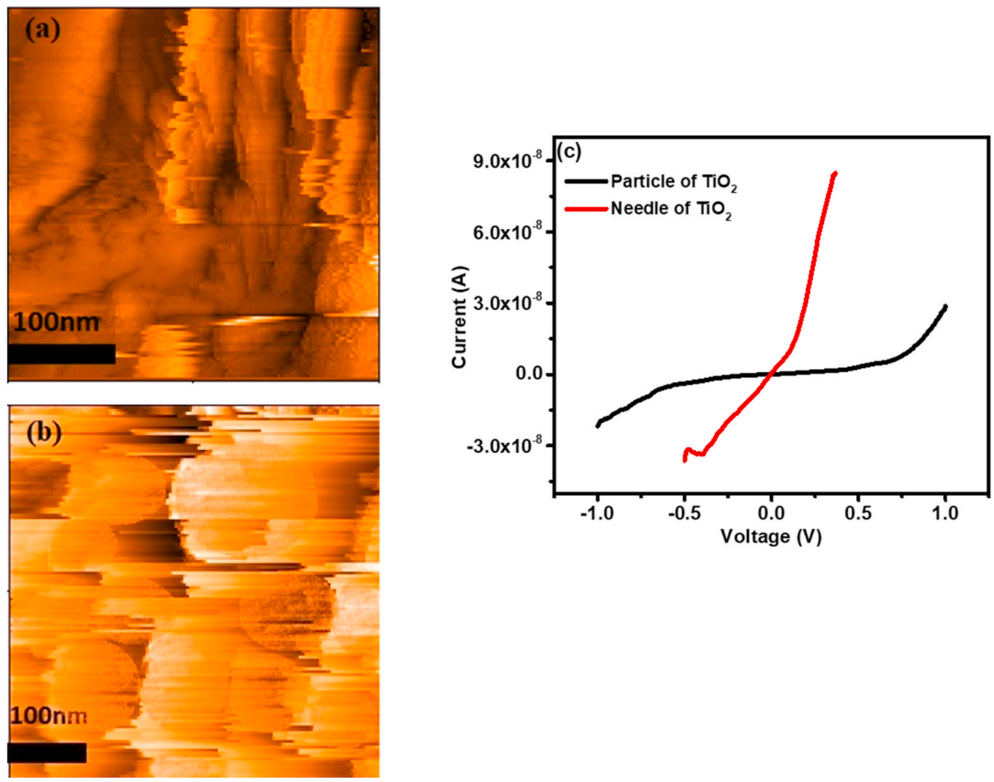

Fig. 4. STM images of **(a)** needle like TiO_2 **(b)** particle like TiO_2. **(c)** IV curves of Particle and Needle of TiO_2.

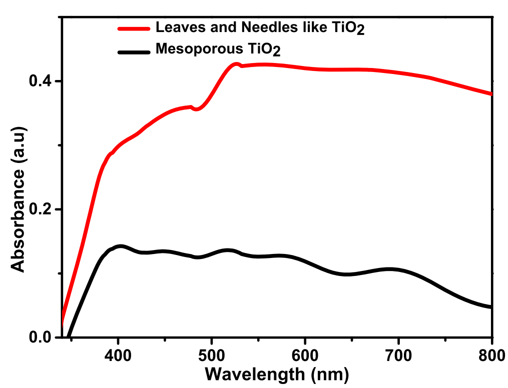

Fig. 5. UV–Visible Absorption spectra of ( ) leaves and needles like TiO_2 (LNT) and ( ) Mesoporous TiO_2 based solar cells.

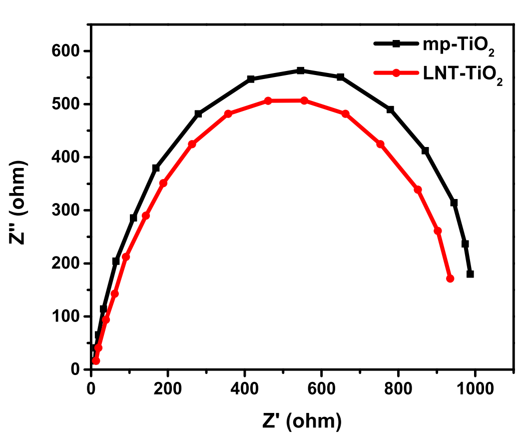

Fig. 6. Nyquist plots of LNT and Mesoporous TiO_2 based solar cells.

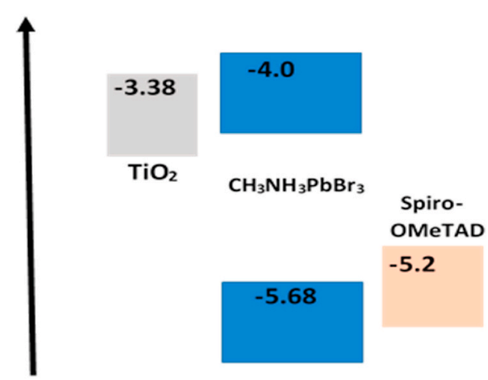

Fig. 7. Diagram of energy levels of each functional layer.

OMeTAD. The energy levels of $CH_3NH_3PbBr_3$ are well aligned with TiO_2 and spiro-OMeTAD for separation and collection of charge carriers.

The current density curves of both devices are shown in Fig. 8. Photovoltaic parameters like open circuit voltage (V_{OC}), short circuit current density (J_{sc}), maximum voltage (V_{max}), maximum current density (J_{max}), fill factor (FF) and power conversion efficiency (PCE) are listed in Table 1.

The values of all these parameters are calculated from IV curves. From Table 1 it is evident that LNT TiO_2 based solar cell has best PCE of 9% with V_{oc} 0.80 V, Jsc 13.12 mA/cm^2 and FF 0.85. Mesoporous TiO_2 based solar cell shows PCE of 6.2% with V_{oc} 0.77 V, J_{sc} 11.21 mA/cm^2 and FF 0.71.

The better performance of LNT TiO_2 based solar cell is due to its leaves and needle like structure. From SEM analysis it is observed that one dimensional needles are randomly dispersed over the leaves throughout the structure. This morphology of TiO_2 plays a vital role to increase the device efficiency. The charge recombination phenomenon tends to lower the efficiency. This factor is overcome by the needles like

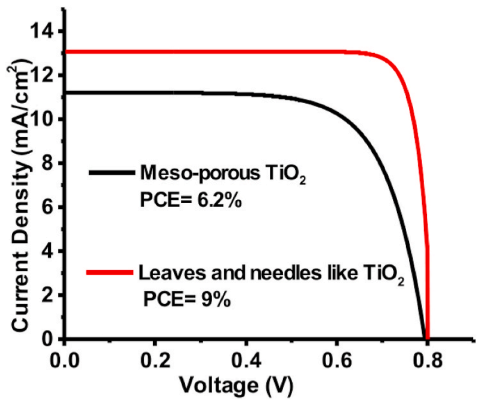

Fig. 8. Dependence of PCE measured by J-V curves on different electron transport layers (ETL). J−V curves of solar cell with Leaves and Needle like TiO_2 (LNT) (red) and Meso-porous TiO_2 (black) as electron transport layer. (For interpretation of the references to color in this figure legend, the reader is referred to the Web version of this article.)

Table 1
Device Performance of $CH_3NH_3PbBr_3$ solar Cells with Different Electron Transport layers (ETL) (Leaves and Needle like TiO_2 (LNT) as ETL, Meso-porous TiO_2 as ETL).

ETL	J_{sc} (mA/cm^2)	V_{oc} (V)	V_{max} (V)	J_{max} (mA/cm^2)	FF	PCE (%)
Meso-porous TiO_2	11.21	0.778	0.622	10	0.71	6.2
Leaves & Needs like TiO^2	13.12	0.801	0.716	12.57	0.85	9

structure of TiO_2. Because the one dimensional nanostructures hinder the charge recombination and increase the charge transport [7,8].

From the STM analysis it is observed that electrical conductivity of needle like structure of TiO_2 is more as compared to TiO_2 particle which also contributes towards increased efficiency.

The leaves like TiO_2 structures help to increase light scattering and trapping by increasing active sites [20,21]. Moreover, this needles and leaves like structure increase the active surface area and area of contact with other layers to provide fast charge transport.

EIS analysis has shown that leaves and needles like TiO_2 structure based solar cell has less interface resistance which leads to fast carrier transport and thus contributes towards better efficiency as compared to mesoporous- TiO_2 structure based solar cell.

4. Conclusions

Two perovskite solar cells with variations in electron transport layers have successfully fabricated. One device has leaves and needle like TiO_2 nanostructure while other device employs mesoporous TiO_2 in electron transport layer. XRD analysis has confirmed the formation of TiO_2. The surface morphology of LNT TiO_2 and mesoporous TiO_2 structures is revealed by TEM, SEM and STM analysis. STM analysis proved that conductivity and electron mobility of needle like structure of TiO_2 is better than particle like structure of TiO_2. Absorption spectra has proved that solar cell based on LNT TiO_2 shows stronger absorption in visible range than solar cell based on mesoporous TiO_2. EIS analysis confirmed that LNT TiO_2 based solar cell shows less interface resistance. The IV analysis has shown that LNT TiO_2 based solar cell shows better PCE of 9% with V_{oc} 0.80, Jsc 13.12 and FF 0.85 while mesoporous TiO_2 based solar cell shows PCE of 6.2% with V_{oc} 0.77, J_{sc} 11.21 and FF 0.71. So it is concluded that better performance of LNT TiO_2 based solar cell is due to its leaves and needle like structure. This structure enhances absorption, scattering and trapping of light and also hinders the charges recombination leading to higher efficiency.

CRediT authorship contribution statement

Hamid Latif: Conceptualization, Methodology, Investigation, Writing - original draft, Supervision. **Zuha Azher:** Methodology. **Syeda Ammara Shabbir:** Methodology, Resources. **Saba Rasheed:** Investigation, Validation. **Erum Pervaiz:** Resources. **Abdul Sattar:** Resources. **Ayesha Imtiaz:** Resources.

Declaration of competing interest

The authors declare that they have no known competing financial interests or personal relationships that could have appeared to influence the work reported in this paper.

Appendix A. Supplementary data

Supplementary data to this article can be found online at https://doi.org/10.1016/j.optmat.2020.110281.

References

[1] L.K. Ono, Y. Qi, S.F. Liu, Progress toward stable lead halide perovskite solar cells, Joule 2 (2018) 1961–1990.
[2] N. Lakhdar, A. Hima, Electron transport material effect on performance of perovskite solar cells based on CH3NH3GeI3, Opt. Mater. (2019) 109517.
[3] G.E. Eperon, S.D. Stranks, C. Menelaou, M.B. Johnston, L.M. Herz, H.J. Snaith, Formamidinium lead trihalide: a broadly tunable perovskite for efficient planar heterojunction solar cells, Energy Environ. Sci. 7 (2014) 982–988.
[4] J. Liu, G. Wang, K. Luo, X. He, Q. Ye, C. Liao, J. Mei, Understanding the role of the electron-transport layer in highly efficient planar perovskite solar cells, ChemPhysChem 18 (2017) 617–625.
[5] P. Su, W. Fu, H. Yao, L. Liu, D. Ding, F. Feng, S. Feng, Y. Xue, X. Liu, H. Yang, Enhanced photovoltaic properties of perovskite solar cells by TiO2 homogeneous hybrid structure, Royal Soc. Open Sci. 4 (2017) 170942.
[6] W.S. Li, T.R. Lin, H.T. Yang, Y.R. Li, K.C. Chuang, Y.S. Li, J.D. Luo, C.S. Hus, H. C. Cheng, Effect of substrate preheating on the photovoltaic performance of ZnO nanorod-based perovskite solar cells, Jpn. J. Appl. Phys. 57 (2018), 06KB03.
[7] X. Ning, J. Huang, S. Li, L. Li, Y. Gu, X. Li, B.H. Kim, Influence of nanobranched growth on photoelectrochemical performance of TiO2 nanotree arrays films, Mater. Sci. Semicond. Process. 94 (2019) 156–163.
[8] J. Qiu, Y. Qiu, K. Yan, M. Zhong, C. Mu, H. Yan, S. Yang, All-solid-state hybrid solar cells based on a new organometal halide perovskite sensitizer and one-dimensional TiO 2 nanowire arrays, Nanoscale 5 (2013) 3245–3248.
[9] Y. Xiao, G. Han, Y. Li, M. Li, J. Wu, Electrospun lead-doped titanium dioxide nanofibers and the in situ preparation of perovskite-sensitized photoanodes for use in high performance perovskite solar cells, J. Mater. Chem. A. 2 (2014) 16856–16862.
[10] S.S. Mali, C.A. Betty, P.S. Patil, C.K. Hong, Synthesis of a nanostructured rutile TiO 2 electron transporting layer via an etching process for efficient perovskite solar cells: impact of the structural and crystalline properties of TiO 2, J. Mater. Chem. A. 5 (2017) 12340–12353.
[11] M. Batmunkh, T.J. Macdonald, C.J. Shearer, M, Y. Wang, M.J. Biggs, I.P. Parkin, T. Nann, J.G. Shapter, Carbon nanotubes in TiO2 nanofiber photoelectrodes for high-performance perovskite solar cells, Adv. Sci. 4 (2017) 1600504.
[12] H. Yu, J. Roh, J. Yun, J. Jang, Synergistic effects of three-dimensional orchid-like TiO 2 nanowire networks and plasmonic nanoparticles for highly efficient mesoscopic perovskite solar cells, J. Mater. Chem. A 4 (2016) 7322–7329.
[13] M. Ye, D. Zheng, M. Lv, C. Chen, C. Lin, Z. Lin, Hierarchically structured nanotubes for highly efficient dye-sensitized solar cells, Adv. Mater. 25 (2013) 3039–3044.
[14] W. Liu, L. Chu, R. Hu, R. Zhang, Y. Ma, Y. Pu, J. Zhang, J. Yang, X.A. Li, W. Huang, Diameter engineering on TiO2 nanorod arrays for improved hole-conductor-free perovskite solar cells, Sol. Energy 166 (2018) 42–49.
[15] M. Yu, Y.Z. Long, B. Sun, Z. Fan, Recent advances in solar cells based on one-dimensional nanostructure arrays, Nanoscale 4 (2012) 2783–2796.
[16] A. Deng, Y. Zhu, X. Guo, L. Zhou, Q. Jiang, Synthesis of various TiO2 micro-/nano-structures and their photocatalytic performance, Materials 11 (2018) 995.
[17] W.Q. Wu, H.L. Feng, H.S. Rao, Y.F. Xu, D.B. Kuang, C.Y. Su, Maximizing omnidirectional light harvesting in metal oxide hyperbranched array architectures, Nat. Commun. 5 (2014) 3968.
[18] H. Huang, L. Pan, C.K. Lim, H. Gong, J. Guo, M.S. Tse, O.K. Tan, Hydrothermal growth of TiO2 nanorod arrays and in situ conversion to nanotube arrays for highly efficient quantum dot-sensitized solar cells, Small 9 (2013) 3153–3160.
[19] C. Hu, X. Zhang, W. Li, Y. Yan, G. Xi, H. Yang, J. Li, H. Bai, Large-scale, ultrathinand (001) facet exposed TiO2 nanosheet superstructures and their applications in photocatalysis, J. Mater. Chem. A 2 (2014) 2040.

[20] C. Liu, J.Y. Tang, H.M. Chen, B. Liu, P.D. Yang, A fully integrated nanosystem of semiconductor nanowires for direct solar water splitting, Nano Lett. 13 (2013) 2989–2992.
[21] J. Di, S. Li, Z. Zhao, Y. Huang, Y.A. Jia, H. Zheng, Biomimetic CNT@ TiO2 composite with enhanced photocatalytic properties, Chem. Eng. J. 281 (2015) 60–68.
[22] Q. Wang, L. Qiu, X. Tan, Z. Liu, S. Gao, R. Wang, Amorphous TiO2 granular nanodisks on porous Ti foam for highly effective solar cells and photocatalysts, J. Taiwan Inst. Chem. E. 102 (2019) 85–91.
[23] Q. Wang, Z. Liu, R. Jin, Y. Wang, S. Gao, SILAR preparation of Bi2S3 nanoparticles sensitized TiO2 nanotube arrays for efficient solar cells and photocatalysts, Separ. Purif. Technol. 210 (2019) 798–803.
[24] L. Qiu, Q. Wang, Z. Liu, Q. Zhao, X. Tian, H. Li, S. Gao, Preparation of 3D TiO2 nanotube arrays photoelectrode on Ti mesh for photoelectric conversion and photoelectrocatalytic removal of pollutant, Separ. Purif. Technol. 207 (2018) 206–212.
[25] K. Indira, U.K. Mudali, T. Nishimura, N. Rajendran, A review on TiO 2 nanotubes: influence of anodization parameters, formation mechanism, properties, corrosion behavior, and biomedical applications, J. Bio Tribo-Corrosion 1 (2015) 28.
[26] X. Zheng, B. Chen, M. Yang, C. Wu, B. Orler, R.B. Moore, K. Zhu, S. Priya, The controlling mechanism for potential loss in CH3NH3PbBr3 hybrid solar cells, ACS Energy Lett. 1 (2016) 424–430.
[27] C. Zhen, T. Wu, R. Chen, L. Wang, G. Liu, H.M. Cheng, Strategies for modifying TiO2 based electron transport layers to boost perovskite solar cells, ACS Sustain. Chem. Eng. 7 (2019) 4586–4618.
[28] J. Zhang, Z. Meng, D. Guo, H. Zou, J. Yu, K. Fan, Hole-conductor-free perovskite solar cells prepared with carbon counter electrode, Appl. Surf. Sci. 430 (2018) 531–538.
[29] C.V. Gopi, M. Venkata-Haritha, K. Prabakar, H.J. Kim, Low-temperature easy-processed carbon nanotube contact for high-performance metal-and hole-transporting layer-free perovskite solar cells, J. Photochem. Photobiol. A Chem. 332 (2017) 265–272.
[30] Z. Liu, T. Shi, Z. Tang, B. Sun, G. Liao, Using a low-temperature carbon electrode for preparing hole-conductor-free perovskite heterojunction solar cells under high relative humidity, Nanoscale 8 (2016) 7017–7023.
[31] A. Kojima, K. Teshima, Y. Shirai, T. Miyasaka, Organometal halide perovskites as visible-light sensitizers for photovoltaic cells, J. Am. Chem. Soc. 131 (2009) 6050–6051.
[32] E. Edri, S. Kirmayer, M. Kulbak, G. Hodes, D. Cahen, Chloride inclusion and hole transport material doping to improve methyl ammonium lead bromide perovskite-based high open-circuit voltage solar cells, J. Phys. Chem. Lett. 5 (2014) 429–433.
[33] S. Ma, T. Ye, T. Wu, Z. Wang, Z. Wang, S. Ramakrishna, C. Vijila, L. Wei, Hollow rice grain-shaped TiO2 nanostructures for high-efficiency and large-area perovskite solar cells, Sol. Energy Mater. Sol. Cells 191 (2019) 389–398.
[34] C. Hu, X. Zhang, W. Li, Y. Yan, G. Xi, H. Yang, J. Li, H. Bai, Large-scale, ultrathin and (001) facet exposed TiO 2 nanosheet superstructures and their applications in photocatalysis, J. Mater. Chem. A 2 (2014) 2040–2043.
[35] M. Ye, et al., Hierarchically structured nanotubes for highly efficient dye-sensitized solar cells, Adv. Mater. 25 (2013) 3039–3044.
[36] U.V. Desai, C.K. Xu, J.M. Wu, D. Gao, Hybrid TiO2-SnO2 nanotube arrays for dye-sensitized solar cells, J. Phys. Chem. C 117 (2013) 3232–3239.
[37] J. Qiu, J, et al., Branched double-shelled TiO2 nanotube networks on transparent conducting oxide substrates for dye sensitized solar cells, J. Mater. Chem. 22 (2012) 23411–23417.
[38] M.D. Ye, X.K. Xin, C.J. Lin, Z.Q. Lin, High efficiency dye-sensitized solar cells based on hierarchically structured nanotubes, Nano Lett. 11 (2011) 3214–3220.
[39] Q. Wang, H. Li, X. Yu, Y. Jia, Y. Chang, S. Gao, Morphology regulated Bi2WO6 nanoparticles on TiO2 nanotubes by solvothermal Sb3+ doping as effective photocatalysts for wastewater treatment, Electrochim. Acta 330 (2020) 135167.